Sensors and Materials, Vol. 38, No. # (2026) 1–20
MYU Tokyo

S & M ####

Payload Measurement of Heavy Vehicles by Measuring Deflection of Leaf Springs for Use of IoT

Shan-Kuo Yang and Kai-Jung Chen*

Department of Mechanical Engineering, National Chin Yi University of Technology, Taichung 41170, Taiwan, R.O.C.

(Received July 1, 2025; accepted June 26, 2026)

Keywords: leaf spring, payload, deflection measurement, strain gage

The overloading of heavy vehicles poses significant risks to road safety and infrastructure. Accurate and real-time payload monitoring is critical for mitigating these risks. In this study, we aim to develop a cost-effective and simplified method for payload estimation in heavy-duty trucks using strain-gage measurements on semi-elliptic leaf springs. A complete system was constructed, incorporating Wheatstone bridge circuitry and signal amplification, followed by experimental calibration and validation under controlled loading conditions. Additionally, theoretical strain-to-load relationships were derived on the basis of classical beam theory and evaluated against experimental results. To overcome the limitations of theoretical estimation, such as nonlinearities and structural uncertainties, a machine learning model using artificial neural networks (ANNs) was developed. A total of 255 data samples were collected from 17 repeated trials across a load range of 0 to 1300 kgf. These were randomly divided into 70% training, 15% validation, and 15% testing subsets. The trained ANN model achieved superior accuracy compared with traditional theoretical approaches. Results indicate that the ANN-based system provides more reliable load predictions than the theoretical strain–load estimation based on classical beam theory, as evidenced by the reduced prediction error (7% compared with 22%), and, owing to its low computational requirement, is suitable for deployment on edge devices such as ESP32 for real-world vehicular applications. The proposed approach offers strong potential for integration into IoT-enabled intelligent transportation systems.

1. Introduction

The overloading of heavy vehicles has long been a significant contributor to road infrastructure damage, shortened vehicle service life, and impaired handling performance. Such overloading can critically increase the risk of accidents, often resulting in severe casualties. Therefore, aside from cautious driving, implementing effective payload control is crucial to prevent traffic incidents and ensure road safety. A fundamental prerequisite for such control is the ability to conveniently and accurately measure the payload of heavy vehicles in real time.

*Corresponding author: e-mail: hskchen5@ncut.edu.tw
https://doi.org/10.18494/SAM5837

ISSN 0914-4935

The truck scale is the most common instrument used to measure vehicle payload. While fixed truck scales offer high precision, their immobility limits their use in on-road enforcement scenarios. Mobile truck scales have been developed to meet field requirements, but their operation is often cumbersome and their accuracy inferior to that of fixed ones. To address these challenges, various research efforts have focused on sensor-based payload estimation.

Roark *et al.*[1] established foundational formulas for stress and strain calculations essential for mechanical load modeling. Fancher *et al.*[2] explored the mechanical behavior of truck leaf springs, forming the basis for many subsequent payload estimation devices. For instance, Nishitani[3] introduced an electromagnetic sensor positioned between the vehicle body and the suspension to derive payload from voltage outputs. Later, Nakazaki *et al.*[4] proposed measuring suspension strain to infer payloads, and many similar techniques followed.

Strain gages are frequently used for such measurements but are vulnerable to harsh environments and exhibit limited service life. Load cells, although more robust, involve significantly more complex installation processes. Regardless of the method, these systems rely on electrical signals, which require signal conditioning and careful wiring.

In contrast, measuring the deflection of leaf springs offers a more straightforward and versatile approach. Numerous methods for deflection measurement have been reported,[5,6] including noncontact solutions utilizing image processing[7] and optical systems.[8] These techniques reduce sensor installation complexity, eliminate wire routing, and minimize maintenance concerns.

In recent years, research attention has expanded to include the use of composite materials for leaf springs,[9] advanced characterizations,[10] and various application domains.[11] Yang *et al.*[12] introduced a neural network model to correct payload estimation errors based on strain-gage measurements. Zheng *et al.*[13] used finite element analysis for composite springs, whereas Venkatesan and Devraj[14] analyzed leaf spring designs for light vehicles. In other studies, material comparisons,[15,16] mechanical spring reviews,[17] and design innovations[18,19] were addressed. In the domain of sensor technology, several recent studies reported in *Sensors and Materials* have resulted in advances in strain-sensing materials and mechanical monitoring. For example, Yamamoto *et al.* developed a liquid-metal embedded strain sensor for soft actuator deformation tracking.[20] Tsai *et al.* employed graphene-enhanced composites to improve the performance of strain sensors on flexible substrates.[21] Shen and Zhu further reported silver nanostructured strain sensors applicable to human motion tracking, highlighting the versatility of novel sensing materials in dynamic mechanical environments.[22]

In parallel, the emergence of AI techniques, particularly artificial neural networks (ANNs), has introduced a powerful means to model complex nonlinear relationships among strain, deflection, and load. ANN-based models can learn from experimental data and generalize load estimations even in the presence of noise or material variability. For example, Nguyen *et al.* employed a backpropagation neural network combined with advanced sensor selection to predict and compensate thermal errors in computer numerical control (CNC) machine tools in real time, demonstrating the capability of ANNs for complex sensor-based prediction tasks.[23] Similarly, deep learning architectures such as convolutional neural networks have been applied in sensor signal processing to extract robust features under noise, confirming the feasibility of AI methods

in sensing environments with nonideal conditions.[24] Moreover, recent work using AI models to process multisensor data (e.g., in real-time fall detection systems) highlights the practical utility of neural network models for mapping heterogeneous sensor inputs to reliable outputs in IoT contexts.[25] These studies support the rationale for adopting ANNs in this work, especially when real-time onboard prediction is required and analytical models are constrained by simplifying assumptions. Despite these efforts, few studies have been aimed at systematically validating deflection-based methods—especially noncontact techniques—for payload estimation under realistic conditions. A comparison of the accuracies of deflection and strain-based methods remains underreported. Additionally, the integration of these methods with IoT platforms for real-time monitoring is still in its infancy.

In this study, we aim to develop a feasible and simplified method for payload measurement in heavy vehicles by analyzing the deflection behavior of leaf springs under load. Both theoretical modeling and practical experiments on semi-elliptic leaf springs are conducted to establish the relationship between deflection and payload. Additionally, an ANN-based model is trained using strain-gage voltage readings to estimate load more robustly under nonlinear and uncertain conditions. The choice of an ANN is motivated by its lightweight computational structure, which is compatible with common IoT microcontrollers such as ESP32. Given that large-scale models are impractical for deployment on such embedded systems, an ANN provides a suitable balance between prediction accuracy and computational efficiency. The proposed hybrid approach combines physical understanding with data-driven modeling, offering a cost-effective, low-complexity alternative to traditional payload sensing techniques. It facilitates future integration with IoT-based monitoring systems, enhancing the practicality of smart logistics, autonomous vehicle management, and real-time overload detection.

2. Materials and Methods

In this section, we introduce the experimental components, strain measurement system, signal conditioning circuitry, loading setup, and the adopted ANN framework for data-driven load estimation. The methodology is divided into three stages: mechanical analysis and testbed design, strain signal calibration and voltage–strain mapping, and ANN training and validation.

2.1 Theoretical basis and structural variations of leaf spring specification

The specimen used in this study is a semi-elliptic leaf spring, which is widely employed in the rear suspension of 3.5-ton trucks. Specifically, it is a commercial component with the part number 48210-0K070, originally designed for the Toyota Hilux Vigo Kun26. Semi-elliptic leaf springs are favored for heavy-duty applications owing to their ability to sustain high loads while allowing substantial deflection.

This spring consists of seven steel strips of progressively decreasing lengths, stacked symmetrically and clamped at the center with a bolt. The ends are mounted on rigid brackets to simulate real-world installation on a truck chassis. During the experiment, a vertical load is applied directly to the spring center, replicating the force exerted by a loaded vehicle. The

vertical deflection at the midpoint is captured using dial indicators, enabling the accurate assessment of deformation under various payload conditions.

The selected leaf spring features a flat cross-sectional design, a common geometry offering a balance between strength and manufacturability. In addition to the cross section, the end structure and spring-eye configuration also affect load distribution and durability. The spring under test adopts standard end loops and eye-type anchoring, consistent with conventional automotive suspension systems. In this study, the specifications of the leaf spring are as follows (Fig 1).

(i) Thickness (t): 8.5 mm
(ii) Width (w): 60 mm
(iii) Total length (L): 1170 mm (active length: 1100 mm)
(iv) Number of leaves (N): 7
(v) Young's modulus (E): 21000 kgf/mm²

According to the Society of Automotive Engineers Handbook,[26] the mechanical behavior of semi-elliptic leaf springs can be accurately described using classical beam theory. In this framework, the stress experienced by the spring is affected by its geometric and material properties, as well as the applied bending moment. Specifically, the relationship between stress, curvature, and moment is governed by the following principles:

(a) Stress is proportional to the product of the leaf thickness (t) and curvature change.
(b) Curvature change is proportional to the ratio of bending moment (M) to the area moment of inertia (I).
(c) Consequently, stress is directly proportional to thickness (t) and bending moment (M), and inversely proportional to the moment of inertia (I).

These relationships form the theoretical basis for correlating applied load with the observed deflection in a leaf spring system. By understanding and quantifying this correlation, it becomes possible to estimate the vehicle's payload through deflection measurements, a key objective of this study.

In addition, the mechanical behavior of semi-elliptic leaf springs can be modeled using classical beam theory. Figure 2 illustrates the deformation of a symmetrical semi-elliptic spring under central loading, along with key analytical formulas.

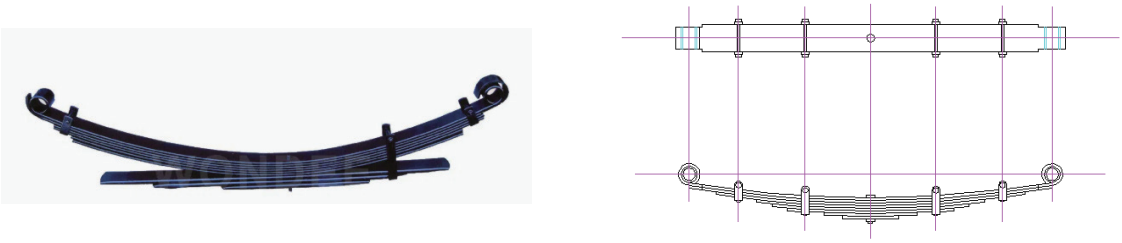

Fig. 1. (Color online) Typical semi-elliptic leaf spring.

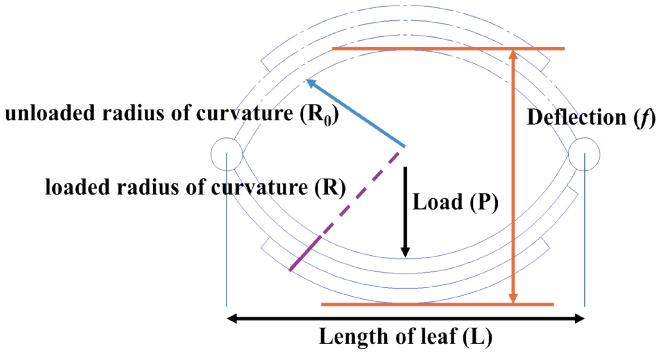

Fig. 2. (Color online) Analytical model and fundamental formulas for a symmetrical semi-elliptic leaf spring under central load. Relationships for deflection, stress, load rate, and strain energy are illustrated on the basis of geometric and material parameters.

Governing Equations

Deflection from geometry:

$$f = \frac{L^2}{8}\left(\frac{1}{R} - \frac{1}{R_0}\right). \tag{1}$$

Stress from strain:

$$S = \frac{E}{2}t\left(\frac{1}{R} - \frac{1}{R_0}\right). \tag{2}$$

Stress from deflection:

$$S = \frac{4Et}{L^2}f\ . \tag{3}$$

Stress from load:

$$S = \frac{3Lt}{2wNt^3}P\,. \tag{4}$$

Load rate (spring stiffness):

$$k = \frac{P}{f} = \frac{8E}{3}\frac{3Nt^3}{L^3}\,. \tag{5}$$

Here, the symbols are defined as follows: L, length of leaf; N, number of leaves; w, width of leaf; t, thickness of leaf; R_0, unloaded radius of curvature (negative value); R, loaded radius of curvature (positive value); E, Young's modulus; f, deflection; S, stress; P, load.

These formulas allow engineers to estimate internal stresses and strains in the leaf spring from measurable geometric or loading parameters. In this study, they are used to validate the strain sensor readings and to establish a load-to-deflection calibration curve.

2.2 Strain sensor configuration and measurement circuit

To measure the strain induced by various loading conditions on the leaf spring, a high-precision foil-type strain gage (SHOWA N11-FA-2-120-23-VSE3) with a nominal resistance of 120 Ω and a tolerance of ±0.3% was employed. Such a gage offers excellent linearity, stability, and repeatability, making it suitable for dynamic mechanical applications in vehicle suspension systems. The detailed specifications of the strain gage are shown in Table 1.

Only one strain gage was used in this study, which was precisely bonded at the midpoint of the leaf spring. This central location experiences the maximum bending strain under symmetric vertical loading. Although the center of the spring is partially constrained by a clamping bolt, the sensor was positioned on a flat region between the bolt flanges to avoid structural interference and ensure consistent strain transmission. This placement allows for a direct correlation between the measured strain and vertical deflection at the spring's most responsive point. Figures 3(a)–3(c) show the leaf spring, the strain gage, and the module of the Wheatstone bridge and amplifier used in this experiment, respectively.

Table 1
Specifications of strain gage.

Gage length (mm)	2
Resistance (Ω)	120 ± 0.3%
Gage factor	2.11 ± 2%
Material	Aluminum
Thermal output	± 2 με/°C

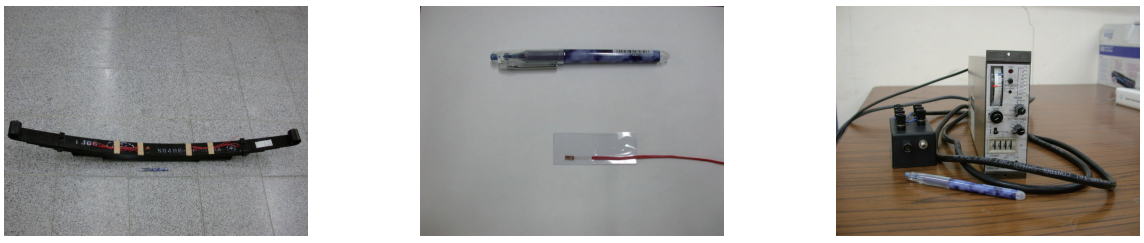

(a) (b) (c)

Fig. 3. (Color online) Devices used in the experiment: (a) leaf spring, (b) strain gage, and (c) module of Wheatstone bridge and amplifier.

To monitor the strain-induced resistance changes in the gage, both DC and AC Wheatstone bridge configurations were initially tested. However, owing to the minimal resistance change in the strain gage during loading (in micro-ohm scale), the output voltage of the bridge was too small to observe directly. Thus, a UA741 operational amplifier was incorporated into the circuit to boost the signal.

The DC Wheatstone bridge was constructed using the strain gage as *RSx* along with three precision resistorsn namely, $RS_1 = RS_2 = 120\ \Omega$ and $RS_3 = 120\ \Omega$, all of which are variable and adjustable for fine-tuning. RS_3 was carefully calibrated to match the initial resistance of *RSx*, making the bridge nearly balanced when unloaded (output voltage $V_G \approx 0$ V). The bridge output was then amplified by the UA741 operational amplifier with a gain configuration of $RS = 500\ \Omega$ and $Rf = 10\ \text{k}\Omega$, providing an amplification factor of approximately 500×. The amplifier was powered by a symmetric dual power supply (±5 V) to allow for positive and negative output swings. The complete circuit configuration of the DC Wheatstone bridge and amplification stage is illustrated in Fig. 4.

Initial calibration was conducted by applying a known preload (2000 kgf) to the spring while adjusting the amplifier gain so that the output voltage reached approximately 5 V. This ensured that subsequent voltage variations due to mechanical loading remained within the amplifier's linear range. The final signal was recorded via a digital acquisition system, and future upgrades may incorporate wireless transmission (e.g., ESP32) to support IoT-based real-time monitoring.

2.3 Loading setup and experimental procedure

A vertical loading rig was designed using a hydraulic jack and a digital force gage to apply controlled loads of up to 1300 kgf. Each loading cycle increased by 100 kgf from 0 to 1000 kgf for calibration, and then extended in 100 kgf increments up to 1300 kgf across 15 sets of full-range trials. At each step, the strain-gage voltage was recorded and later converted using the previously derived equation.

Each load point was held for 5 min to ensure mechanical stabilization before unloading. A total of 255 data points were collected. Among them, 70% were used for ANN training, 15% for validation, and 15% for testing.

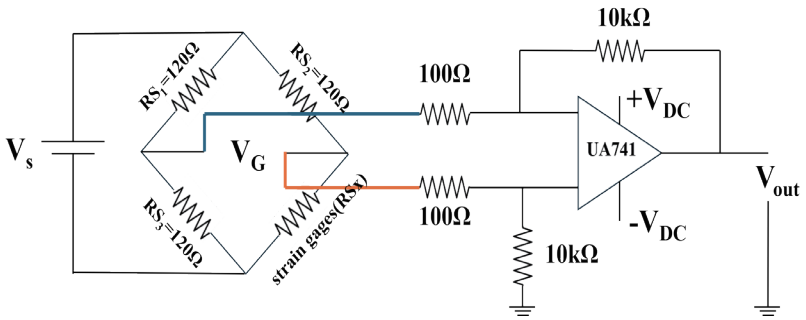

Fig. 4. (Color online) Circuit diagram of the DC Wheatstone bridge connected to the UA741 operational amplifier.

At each load step, strain data were collected from both strain gages positioned at 195 mm from the center, while vertical deflection was simultaneously measured using a precision dial indicator placed at the midpoint of the spring.

The output voltage from the Wheatstone bridge circuits was logged through a data acquisition system, calibrated in advance to convert voltages into corresponding strain values (με). These measurements were repeated three times at each load level to ensure data consistency and minimize experimental uncertainty.

Ambient temperature was monitored and maintained within ±1 °C to mitigate thermal drift effects. All instrumentation, including power supply and amplifiers, was warmed up for at least 30 min prior to data collection to ensure steady-state operation.

This procedure allows accurate mapping between the applied payload and the corresponding strain or deflection, forming the basis for regression modeling and payload estimation presented in subsequent sections. Figures 5(a) and 5(b) show the leaf spring before and after loading in the experimental setup, respectively.

3. Experimental Results

3.1 Strain measurement and system calibration

In this study, strain measurement was conducted using a foil-type strain gage (SHOWA N11-FA-2-120-23-VSE3) that was centrally mounted on the main leaf of a semi-elliptic leaf spring. The gage, with a nominal resistance of 120 Ω and a tolerance of ±0.3%, was connected to a DC Wheatstone bridge to detect small resistance changes caused by mechanical deformation. To match the sensor's baseline resistance and minimize offset, a precision variable resistor R3 in the bridge was initially adjusted to 120.1 Ω. This adjustment ensured that the output voltage of the bridge circuit remained near zero before loading began, providing a reliable baseline for calibration.

(a) (b)

Fig. 5. (Color online) Experimental setup: (a) before and (b) after loading.

Before formal calibration, a preliminary verification procedure was performed. The system underwent five cycles of light loading and unloading. After each unloading, a waiting period of 5 min was introduced to allow the spring to return to its undeformed state. During this process, the average amplifier output voltage was recorded as approximately 0.0196 V, with a standard deviation of ±0.0271 V. This near-zero mean output confirmed the system's electrical and mechanical stabilities under its unstrained condition. The detailed voltage measurements under the no-load condition are summarized in Table 2.

The formal calibration was carried out by applying a reference load of 800 kgf to the leaf spring center while monitoring the corresponding output voltage. The load was gradually applied and maintained for 5 min to ensure mechanical stabilization. Subsequently, the load was removed, and the system was again allowed to return to its original state for another 5 min. This load–unload cycle was repeated five times, with voltage measurements recorded under both the zero-load and full-load conditions. Averaged over the five cycles, the measured output voltage for the zero-load state was 0 V, whereas the full-load state (corresponding to a strain of approximately 2000 με) produced an output of 2.685 V.

Using these two calibration points, we performed a linear regression to derive a conversion equation between the measured voltage (V) and strain (ε, in microstrain). The resulting equation is

$$\varepsilon = 741.02 \times V \,, \tag{6}$$

where ε is the calculated strain (με) and V is the measured voltage (V). The corresponding calibration curve and linear regression result are shown in Fig. 6.

This linear model exhibited high consistency across repeated measurements and was subsequently used to convert voltage outputs from all the following experiments into meaningful strain values. The reliability of this calibration confirms the suitability of the designed measurement system for further payload estimation tasks.

In this study, the deflection of the semi-elliptic leaf spring is modeled using a simplified single-beam approximation, assuming that the multi-leaf spring stack behaves like a uniform elastic beam with consistent cross-sectional properties. This model neglects several real-world complexities, such as interleaf friction, varying contact conditions between individual leaves, nonlinear stiffness behavior, and variations in leaf geometry. These simplifications were adopted

Table 2
Repeated voltage measurements of Wheatstone bridge at RS3 ≈ 120.1 Ω under no-load condition.

No.	Precision variable resistor R3 (Ω)	Measured voltage (V)
1	120.10	0
2	120.07	0
3	120.14	0.0214
4	120.12	0.0766
5	120.11	0
Mean value	120.10	0.0196

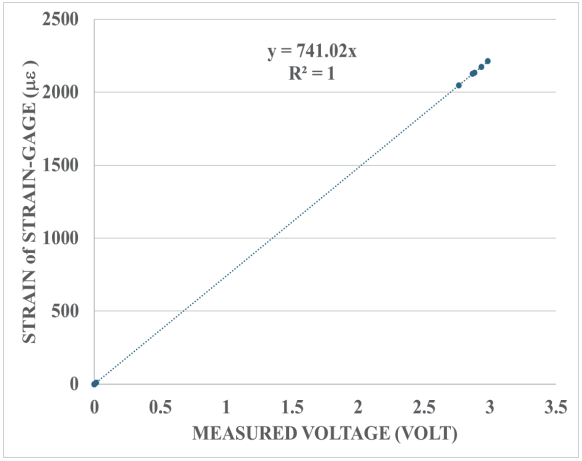

Fig. 6. (Color online) Calibration curve of strain gage: relationship between measured voltage and corresponding strain with linear regression.

to provide a tractable baseline for initial strain–load correlation and to allow the early validation of the sensing concept.

However, these idealized assumptions contribute to modeling inaccuracies. For example, the calculated strain under a full reference load using this single-beam model exhibited an average deviation of 22% compared with the actual strain measured by the strain gage. This discrepancy stems primarily from the unmodeled interactions among leaf interfaces and nonlinear deformation mechanisms in real steel springs. Despite this limitation, the simplified model provides a valuable baseline for validating the feasibility of using leaf spring strain for payload estimation and serves as the foundation for data-driven compensation using ANN modeling in subsequent sections.

3.2 Payload estimation and theoretical validation

To evaluate the performance and consistency of the developed measurement system, a controlled load test was conducted by applying vertical loads ranging from 0 to 1000 kgf in 100 kgf increments at the center of the leaf spring. At each load level, the corresponding output voltage from the strain gage was measured. This voltage was then converted into strain using the previously established calibration equation. To verify measurement stability and reproducibility, the entire loading sequence was repeated five times under identical experimental conditions.

Table 3 shows the raw voltage outputs collected from five repetitions across 11 loading levels. The average and standard deviation at each level are also presented. The results indicate relatively small standard deviations (e.g., 0.0206 V at 1000 kgf and 0.0338 V at 700 kgf), which suggest good repeatability of the strain measurements. However, slightly higher variations were observed at intermediate loads such as 150 and 300 kgf, with standard deviations of 0.2795 and 0.2716 V, respectively. These fluctuations may result from initial settling behaviors or sensor hysteresis during light loading.

Table 3
Measured voltages from repeated strain-gage outputs at incremental loading (0–1000 kgf).

Load (kgf)	No. 1 (V)	No. 2 (V)	No. 3 (V)	No. 4 (V)	No. 5 (V)	Mean (V)	SD (V)
0	0.0436	0.0000	0.0611	0.0000	0.0068	0.0223	0.0231
50	0.2743	0.4174	0.3284	0.1478	0.3778	0.3091	0.0857
100	0.7163	0.7543	0.7954	0.5254	0.6225	0.6828	0.0888
150	0.7496	1.5594	1.3623	0.8376	1.1130	1.1244	0.2795
200	1.2721	1.3493	1.2817	1.2619	1.4690	1.3268	0.0707
300	1.6948	1.2890	2.1618	1.5641	1.9115	1.7242	0.2716
400	1.8068	1.9015	1.7442	1.8143	1.8239	1.8181	0.0458
500	2.5629	2.2560	1.8770	2.1282	2.1803	2.2009	0.2019
600	2.3897	2.6261	2.5755	2.1466	2.2702	2.4016	0.1649
700	2.5726	2.5853	2.6001	2.6231	2.6778	2.6118	0.0338
800	2.9326	2.8934	2.9526	2.9122	2.9511	2.9284	0.0208
900	3.0440	3.3426	3.3529	2.9485	3.0339	3.1444	0.1546
1000	3.5085	3.4870	3.4908	3.5421	3.4787	3.5014	0.0206

To validate the effectiveness of the strain-based load estimation method, the voltage signals measured during the repeated loading experiments were converted into microstrain (με) values using the calibrated linear relationship. The resulting strain values corresponding to each load level (0–1000 kgf in 100 kgf increments) are shown in Table 4. As with the raw voltage data, five repetitions were conducted and the mean and standard deviation were calculated to evaluate repeatability.

The resulting strain data revealed consistent and proportional increases with applied load. For example, the mean strain at 0 kgf was 16.52 με, which approaches the ideal zero-load condition, while at 1000 kgf, the average strain reached 2594.62 με. Low standard deviations at the higher load levels (e.g., 15.25 με at 1000 kgf) suggest excellent repeatability and sensor stability under heavy load. Conversely, higher variations were observed at lower or intermediate loads (e.g., 207.11 με at 150 kgf and 201.23 με at 300 kgf), possibly caused by mechanical settling, hysteresis, or friction within the suspension system during initial load transitions.

As shown in Fig. 7(a), the measured voltage exhibits a strong linear correlation with the applied load. A linear regression of the average voltage values across five trials yields the relationship

$$V = 0.0032 \times P + 0.437 \left(R^2 = 0.9608 \right). \tag{7}$$

This high coefficient of determination indicates a well-defined voltage response to increasing payload. The consistency among the five trials also demonstrates the reliability of the strain gage and amplification system under repetitive loading conditions.

By converting the measured voltages into strain values using the calibration function, the load–strain relationship is further clarified in Fig. 7(b). The averaged results again show excellent linearity, and the derived regression equation is

Table 4
Converted strain (με) values from repeated strain-gage outputs under incremental loading (0–1000 kgf).

Load (kgf)	No. 1 (με)	No. 2 (με)	No. 3 (με)	No. 4 (με)	No. 5 (με)	Mean (με)	SD (με)
0	32.31	0.00	45.28	0.00	5.04	16.52	17.10
50	203.26	309.30	243.35	109.52	279.96	229.08	63.49
100	530.79	558.95	589.41	389.33	461.29	505.95	65.81
150	555.47	1155.55	1009.49	620.68	824.76	833.19	207.11
200	942.65	999.86	949.77	935.09	1088.56	983.19	52.37
300	1255.88	955.17	1601.94	1159.03	1416.46	1277.70	201.23
400	1338.87	1409.05	1292.49	1344.43	1351.55	1347.28	33.95
500	1899.16	1671.74	1390.89	1577.04	1615.65	1630.90	149.65
600	1770.82	1945.99	1908.50	1590.67	1682.26	1779.65	122.16
700	1906.35	1915.76	1926.73	1943.77	1984.30	1935.38	25.06
800	2173.12	2144.07	2187.94	2158.00	2186.82	2169.99	15.44
900	2255.66	2476.93	2484.57	2184.90	2248.18	2330.05	114.57
1000	2599.87	2583.94	2586.75	2624.77	2577.79	2594.62	15.25

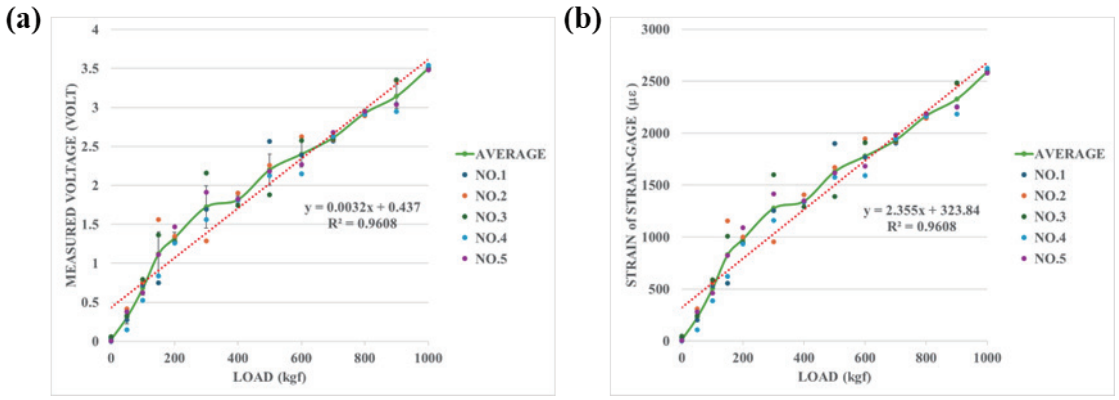

Fig. 7. (Color online) Measured voltage (a) and calculated strain versus (b) applied load, showing five repeated trials, average curves, and linear regression lines based on calibration.

$$\varepsilon = 2.355 \times P + 323.84 \left(R^2 = 0.9608 \right). \tag{8}$$

This linear relationship confirms the suitability of the system for payload estimation via strain measurement. It also provides a robust basis for theoretical comparisons and error analysis in subsequent experiments.

To assess the feasibility of using the measured strain for estimating the applied payload, the theoretical relationship between strain and load was reversed. By rearranging the classical beam-based expression derived from semi-elliptic leaf spring theory, the applied load (P_e) can be estimated directly from the measured strain (ε) as shown below.

$$P_e = \frac{2wNt^2E\varepsilon}{3L} \tag{9}$$

Here, P_e is the estimated load (kgf), ε is the measured strain (με), L is the effective length of the leaf spring (1170 mm), w is the width of each leaf (60 mm), N is the number of leaves (7), t is the thickness of each leaf (8.5 mm), and E is Young's modulus (21000 kgf/mm²).

Using this equation, we calculated the predicted payload values for all the measured strain values from the previous dataset. The results are summarized in Table 5, which shows the predicted loads for each of the five trials, the mean, and the standard deviation.

The findings suggest that this analytical model yields good agreement with the actual applied load, particularly at higher loads (e.g., error < 1% at 1000 kgf). The standard deviation of predicted values also decreases with increasing load, reaching only ±5.54 kgf at 1000 kgf. However, at lower loads, deviations become more pronounced owing to signal instability, strain-gage sensitivity limits, and possible structural hysteresis. For example, at 150 kgf, the standard deviation reaches 75.20 kgf, which implies that low-load accuracy is insufficient for practical use.

Using the rearranged theoretical equation [Eq. (9)], we applied the experimentally measured strain data from Fig. 7 to estimate the corresponding load values. However, when comparing the estimated results with the actual applied loads, it was evident that the theoretical model consistently underestimated the true payload across most loading conditions.

For example, at the actual load of 1000 kgf, the measured mean strain was approximately 2594.62 με. Substituting this value into the model yields the estimated load as

$$P_e = \frac{2\times 60\times 7\times 8.5^2\times 21000\times 2594.62\times 10^{-6}}{3\times 1170} \approx 942.11\text{kgf}\,. \tag{10}$$

Table 5
Estimated payload (kgf) calculated from measured strain using Eq. (9).

Load (kgf)	No. 1 Predicted load (kgf)	No. 2 Predicted load (kgf)	No. 3 Predicted load (kgf)	No. 4 Predicted load (kgf)	No. 5 Predicted load (kgf)	Mean (kgf)	STD (kgf)
0	11.73	0.00	16.44	0.00	1.83	6.00	6.21
50	73.80	112.31	88.36	39.77	101.65	83.18	23.05
100	192.73	202.96	214.02	141.37	167.49	183.71	23.90
150	201.69	419.58	366.55	225.37	299.47	302.53	75.20
200	342.28	363.05	344.86	339.53	395.26	357.00	19.01
300	456.01	346.83	581.67	420.85	514.32	463.93	73.07
400	486.15	511.63	469.31	488.17	490.75	489.20	12.33
500	689.59	607.01	505.04	572.63	586.65	592.18	54.34
600	642.99	706.59	692.98	577.58	610.83	646.19	44.36
700	692.20	695.62	699.60	705.79	720.51	702.74	9.10
800	789.06	778.52	794.45	783.57	794.04	787.93	5.61
900	819.04	899.38	902.15	793.34	816.32	846.05	41.60
1000	944.02	938.23	939.26	953.06	936.00	942.11	5.54

This corresponds to a relative error of

$$Error\ \% = \frac{942.11 - 1000}{1000} \times 100\% \approx -6\% . \tag{11}$$

The results of the overall error analysis for each trial and load level are shown in Table 6. Although the model performs well under high loads (e.g., <6% error at 1000 kgf), the error becomes significant at low loads owing to increased signal noise, circuit instability, and the limited sensitivity of the strain-gage circuit.

The consistent overestimation suggests that while the theoretical model is structurally valid, it may not fully account for factors such as residual stress, assembly friction, nonuniform leaf stiffness, or strain-gage installation offset. Therefore, a direct inverse calculation from measured strain to payload using the beam-based model introduces notable inaccuracies in this specific leaf spring configuration.

Classical beam theory, while valuable in establishing foundational relationships, fails to capture the complex nonlinearities present in real-world leaf spring systems, such as material inhomogeneity, assembly friction, residual stress, and sensor installation offsets. These factors contribute to deviations between theoretical estimates and actual responses.

To address this limitation, a data-driven approach utilizing machine learning algorithms—such as ANNs—can be implemented. By training the model on experimentally collected strain-load datasets, the AI system can learn the underlying nonlinear mappings and compensate for hidden variables. This enables a more accurate payload prediction even in the presence of system noise or uncertainties.

Table 6
Relative errors of predicted load values based on theoretical strain model (%).

Load (kgf)	Error of No. 1 Predicted load (%)	Error of No. 2 Predicted load (%)	Error of No. 3 Predicted load (%)	Error of No. 4 Predicted load (%)	Error of No. 5 Predicted load (%)	Mean (%)	STD (%)
0	—	—	—	—	—	—	—
50	48	125	77	-20	103	66	46
100	93	103	114	41	67	84	24
150	34	180	144	50	100	102	50
200	71	82	72	70	98	78	10
300	52	16	94	40	71	55	24
400	22	28	17	22	23	22	3
500	38	21	1	15	17	18	11
600	7	18	15	-4	2	8	7
700	-1	-1	0	1	3	0	1
800	-1	-3	-1	-2	-1	-2	1
900	-9	0	0	-12	-9	-6	5
1000	-6	-6	-6	-5	-6	-6	1

3.3 Load estimation using ANN

To overcome the limitations of traditional theoretical models in accurately estimating load from strain-gage signals, particularly under nonlinear or nonideal mechanical responses, we employed an ANN approach. Unlike analytical equations that require accurate knowledge of spring geometry and stress distribution, the ANN directly models the mapping from voltage signals to applied load, providing a data-driven solution suitable for real-world applications.

A total of 255 data points were collected from 17 repeated experimental trials, covering load increments from 0 to 1300 kgf, following the same experimental protocol as described in previous sections. For each load step, the amplified voltage output from the strain-gage circuit was recorded, forming a voltage-load dataset for ANN training. The data were randomly divided into 70% training, 15% validation, and 15% testing subsets.

The network structure adopted a single hidden layer with 10 neurons, and training was performed using the Levenberg–Marquardt backpropagation algorithm. The architecture of the developed ANN model is shown in Fig. 8(a). The training performance curve is presented in Fig. 8(b), where the ANN reached its best validation performance [mean squared error (*MSE*) = 4403.88] at epoch 32. The error distribution was evaluated using the histogram in Fig. 8(c),

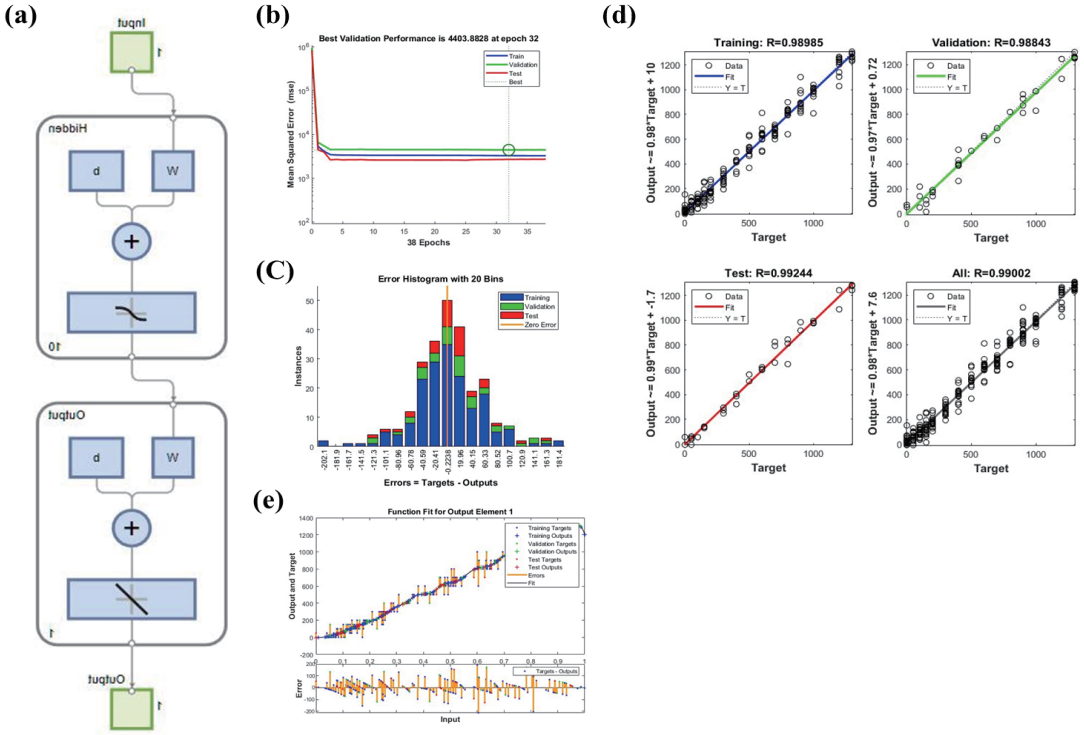

Fig. 8. (Color online) Architecture and performance of the developed ANN model. (a) ANN model structure with one hidden layer. (b) Performance curve showing best validation at epoch 32. (c) Error histogram showing symmetric distribution centered near zero. (d) Regression plots for training, validation, testing, and all datasets. (e) Function fit and residual error plot showing model generalization.

which exhibits a near-symmetric distribution centered at zero, with most prediction errors within ±100 kgf. The regression results are illustrated in Fig. 8(d), showing high correlation coefficients across all subsets: R = 0.98985 (training), 0.98843 (validation), 0.99244 (testing), and 0.99002 overall. Finally, the function fit and residual plot in Fig. 8(e) demonstrates no significant bias or overfitting, confirming the ANN model's generalization capability.

To evaluate practical applicability, the trained ANN model was tested against an additional 48 validation samples. As shown in Fig. 9(a), the ANN results closely followed the target values and remained mostly within the ±2σ confidence bounds. In contrast, the results of theoretical estimation using Eq. (10) [Fig. 9(b)] exhibited more significant deviations, particularly in the mid-to-high load range.

As summarized in Table 7, the ANN model achieved a mean estimated load of 586.76 ± 326.09 kgf compared with the actual measured load of 592.39 ± 333.76 kgf, yielding a relative error of only 7%. The theoretical model, by contrast, produced a larger deviation (22% error, 609.56 ± 305.31 kgf). These results confirm that the ANN approach is more accurate and robust for payload estimation in leaf spring systems.

In contrast to the theoretical approach, which assumes idealized uniform deformation and material behavior, the ANN model captures the nonlinear characteristics and system noise inherent in the strain–voltage–load relationships. This demonstrates the ANN's superior capability in modeling complex real-world load estimation tasks under various mechanical conditions.

While the ANN model functions as a data-driven estimator, its improved performance can be physically interpreted in the context of real leaf spring behavior. In practical suspension systems, the strain–load relationship deviates from ideal beam theory owing to several nonlinear factors, including interleaf friction, residual stress from manufacturing and assembly, the material hysteresis of spring steel, and local strain-gage installation offsets. These effects result in load-dependent stiffness variations and asymmetric loading–unloading responses that are difficult to explicitly formulate using classical analytical models.

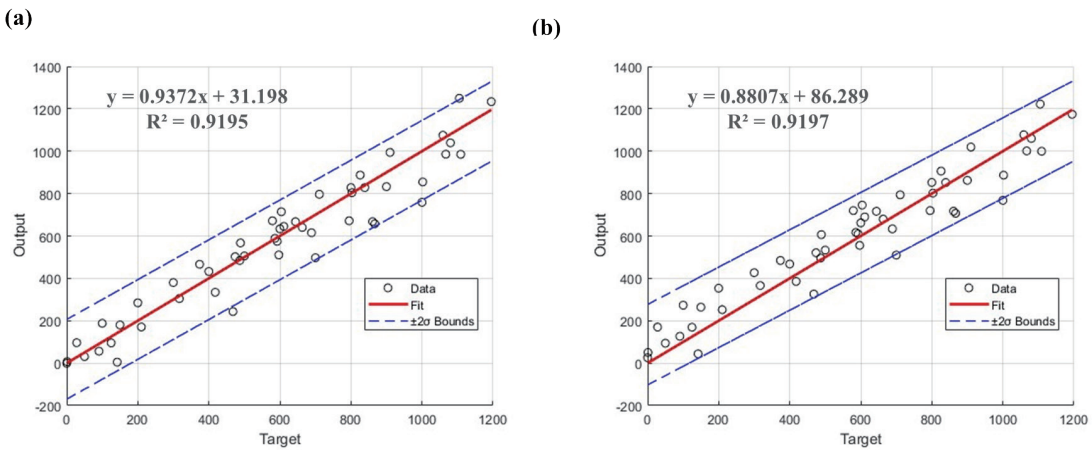

Fig. 9. (Color online) Results of (a) ANN prediction and (b) theoretical calculation using Eq. (10).

Table 7
Load estimation accuracies of ANN prediction and theoretical calculation.

Mean ± STD of load (kgf)	Mean ± STD of measured voltage (V)	Mean ± STD of load from ANN-model predictions (kgf)	Error of ANN-model predictions	Mean ± STD of load from theoretical calculations (kgf)	Error of theoretical calculations
592.39 ± 333.76	2.26 ± 1.13	586.76 ± 326.09	7%	609.56 ± 305.31	22%

By training on experimentally measured voltage–load data, the ANN implicitly learns these nonlinear mappings and compensates for the combined effect of mechanical hysteresis and structural nonuniformity. As a result, the ANN effectively corrects the systematic bias observed in the theoretical inverse calculation, particularly in the mid-to-high load range. Although the ANN does not provide explicit physical parameters, its predictions remain consistent with the observed mechanical behavior, thereby offering a practical and physically meaningful enhancement over simplified beam-based models for real-world payload estimation.

4. Discussion

In this study, we presented a strain-gage-based method for estimating payload on a leaf spring suspension system and explored both theoretical modeling and ANN-based prediction approaches. Several key findings and implications can be derived from the experimental results.

First, the calibration of the strain gage and measurement circuit demonstrated high linearity and stability. The use of a dedicated Wheatstone bridge with precise resistors and independent UA741 amplification ensured minimal signal drift and accurate strain-to-voltage conversion. As shown in Table 2, the initial zero-load condition returned near-zero voltage outputs with low standard deviation, confirming the system's baseline repeatability. The linear calibration between strain and voltage also enabled reliable conversion during subsequent testing.

In the second phase, theoretical strain calculations based on classical semi-elliptic leaf spring models were used to validate experimental data. Although the general trend was consistent, the direct inversion from the measured strain to payload showed systematic underestimation errors averaging around −6% at high loads (as summarized in Table 6). This discrepancy likely results from unaccounted factors such as leaf layer friction, residual stress, and imperfect strain-gage positioning. Thus, while the theoretical model remains useful for general estimation, its application is limited under nonideal conditions.

To address these limitations, the ANN-based model was trained using the voltage–load dataset without requiring conversion to strain. This approach allowed the network to learn the nonlinear mappings directly from the measured signals. The ANN achieved excellent predictive performance, with regression correlation coefficients exceeding 0.99 and most errors within ±100 kgf (see Fig. 8). Compared with the theoretical model, the ANN produced a lower mean absolute error (7% vs 22%, Table 7) when applied to new validation data.

Furthermore, the choice of an ANN is particularly practical for IoT-based implementation. Lightweight neural networks, such as the one used in this study, can be deployed on microcontrollers such as ESP32, which are commonly used in embedded vehicle systems. The low computational complexity and high inference speed of ANN models make them ideal for real-time onboard payload monitoring.

Although the current experimental validation was conducted under static loading conditions, it is acknowledged that dynamic driving environments introduce additional challenges such as vibration-induced signal fluctuations and transient loading effects. To enhance the robustness of the proposed system for real-world vehicular use, future work may incorporate signal smoothing techniques (e.g., moving average and Kalman filtering), sensor fusion with accelerometers for dynamic compensation, and real-time denoising algorithms. The compact nature of the ANN model further supports deployment on embedded IoT platforms with edge computing capabilities. These extensions are essential steps toward enabling real-time load monitoring under dynamic driving conditions.

5. Conclusions

In this study, we proposed a practical, cost-effective method for payload estimation in heavy vehicles by analyzing the strain response of a semi-elliptic leaf spring under load. Both theoretical modeling and experimental testing were conducted to evaluate the accuracy and applicability of the proposed measurement system. Although classical beam-based equations provided a baseline for load estimation, the results revealed that these equations tend to overestimate the payload, particularly owing to structural complexity, residual stresses, and sensor-related uncertainties.

To overcome these limitations, an ANN model was developed using experimentally measured voltage–load datasets. The ANN achieved high prediction accuracy, with regression values exceeding 0.99 and a significant reduction in estimation error compared with the theoretical approach. Furthermore, when tested with independent verification data, the ANN predictions closely followed the target load values and remained within a $\pm 2\sigma$ confidence interval.

Importantly, the ANN model can be implemented using lightweight microcontrollers such as ESP32 with MicroPython, enabling seamless integration into vehicle-mounted IoT systems. This paves the way for real-time overload monitoring and intelligent fleet management. The findings of this research provide a feasible pathway for transitioning from theory-based load prediction to data-driven, deployable sensing solutions for smart logistics applications.

References

1 R. J. Roark, W. C. Young, and R. Plunkett: J. Am. Soc. Mech. Eng. **43** (1976) 522. https://doi.org/10.1115/1.3423917
2 P. S. Fancher, , R. D. Ervin, and C. B. Winkler: SAE Tech. Papers (1980) 800905. https://doi.org/10.4271/800905
3 K. Nishitani: Electromagnetic-Type Load Weighing Apparatus, United States Patent 5243 (1993) 146.
4 Y. Nakazaki, H. Aoshima, N. Takahashi, Y. Atagi, Y. Yasuda: Load Measuring Device for a Vehicle, United States Patent 5684 (1997) 254.

5 J. G. Webster: Sensors and Signal Conditioning (Wiley, New York,1991).
6 J. R. Carstens: Electrical Sensors and Transducers (Prentice Hall, Englewood Cliffs, 1993).
7 V. Batagelj, J. Bojkovski, J. Drnovsek, and I. Pusnik: IEEE Trans. Instrumentation and Measurement **50** (2001) 6. https://doi.org/10.1109/19.982951
8 S. Pavageau, R. Dallier, N. Servagent, and T. Bosch: Meas. Sci. Technol. **14** (2003) 2121. https://doi.org/10.1088/0957-0233/14/12/011
9 M. S. Mahnood and R. Davood: Compos. Struct. **60** (2003) 317. https://doi.org/10.1016/S0263-8223(02)00349-5
10 J. B. Hoyle: Proc. Institution of Mechanical Engineers, Part D: J. Automob. Eng. **218** (2004) 3. https://doi.org/10.1243/095440704322955795
11 J. P. Meijaard, D. M. Brouwer, and J. B. Jonker: Multibody Syst. Dyn. **23** (2010) 77. https://doi.org/10.1007/s11044-009-9172-4
12 S. K. Yang, T. S. Liu, and Y. C. Cheng: Measurement. **41** (2008) 5. https://doi.org/10.1016/j.measurement.2007.07.003
13 Z. Yinhuan, X. Ka, and H. Zhigao: 2011 6th Int. Conf. Computer Science & Education (ICCSE) (IEEE, 2011). https://doi.org/10.1109/ICCSE.2011.6028643
14 M. Venkatesan and D. M. Devraj: Int. J. Modern Eng. Res. **2** (2012) 213. https://www.ijmer.com/papers/vol2_issue1/AH021213218.pdf
15 S. D. Rathod, D. S. Shah, and S. A. Ban: Int. J. Mech. Prod. Eng. Res. Dev. **3** (2013) 1. https://doi.org/10.1016/j.sna.2012.08.031
16 K. S. Naresh: IUP J. Mech. Eng. **4** (2018) 2579. https://www.irjet.net/archives/V3/i5/IRJET-V3I5538.pdf
17 N. Singh: Int. J. Adv. Eng. Res. Sci. **115** (2013) 112. https://www.academia.edu/download/37173645/395.pdf
18 M. C. Madhava and G. Deepak: Int. J. Eng. Res. **5** (2016)1244. https://www.academia.edu/download/47842290/23.pdf
19 L. Zhao, Y. Yu, and C. Zhou: Int. J. Eng., Trans. B **31** (2018) 204. https://doi.org/10.5829/ije.2018.31.02b.03
20 S. Yamamoto, H. Ishizuka,, T. Hiraki, S. Ikeda, and O. Oshiro: Sens. Mater. **36** (2024) 2209. https://doi.org/10.18494/SAM5009
21 T. Y. Tsai, S. Y. Su, S. L. Tu, and T. H. Chen: Sens. Mater. **37** (2025) 1853. https://doi.org/10.18494/SAM5501
22 Y. Shen and Q. Zhu: Sens. Mater. **37** (2025) 2223. https://doi.org/10.18494/SAM5649
23 D. K. Nguyen, H. C. Huang, and Z. M. Hsu: Sens. Mater. **37** (2025) 5201. https://doi.org/10.18494/SAM5879
24 J. Ding, and M. C. Hsieh: Sens. Mater. **37** (2025) 2489. https://doi.org/10.18494/SAM5558
25 Y. S. Chang, and G. Y. Lin: Sens. Mater. **37** (2025) 1639. https://doi.org/10.18494/SAM5419
26 Society of Automotive Engineers: Spring Committee Supplement. Manual on design and application of leaf springs--SAE HS J788: Report of the Spring Committee (Warrendale, PA : Society of Automotive Engineers. 1982).

About the Authors

Shang-Kuo Yang received his B.S. degree in 1982 and M.S. degree in 1985 in automatic control engineering from Feng Chia University, and his Ph.D. degree in 1999 in mechanical engineering from National Chiao Tung University, Taiwan. From 1985 to 1991, he was an assistant researcher and an instrumentation system engineer of the Flight Test Group, Aeronautic Research Laboratory, Zhong Shan Institute of Science and Technology, Taiwan. Since 1991, he has been with the Department of Mechanical Engineering at National Chin Yi University of Technology, Taiwan. His research interests are in reliability engineering, data acquisition system, biomedical engineering (cardiac pacemakers, patient nursing monitoring, otoliths restoration, and drunk-driving prevention), and automation.
(skyang@ncut.edu.tw)

Kai-Jung Chen is an accomplished individual with a bachelor's degree in engineering (2010) and a master's degree in biomechanical engineering (2012) from National Cheng Kung University in Taiwan, and a Ph.D. degree in engineering from the University of Liverpool, UK (2019). From 2014 to 2019, he played a pivotal role in the Biomechanical Engineering Group at the University of Liverpool, focusing on precision ophthalmic equipment development. Since 2020, he has been a faculty member in the Department of Mechanical Engineering at National Chin-Yi University of Technology, Taiwan. His diverse research interests include computational biomechanics, medical assistive device development, big data and AI technology, and semiconductor and brittle material processing. (hskchen5@ncut.edu.tw)